Monthly Notices
of the
ROYAL ASTRONOMICAL SOCIETY

MNRAS **460,** 3669–3678 (2016)
Advance Access publication 2016 May 12

doi:10.1093/mnras/stw1125

Radio luminosity function of brightest cluster galaxies

Z. S. Yuan,[1,2] J. L. Han[1]★ and Z. L. Wen[1]

[1]*National Astronomical Observatories, Chinese Academy of Sciences, 20A Datun Road, Chaoyang District, Beijing 100012, China*
[2]*School of Astronomy, University of Chinese Academy of Sciences, Beijing 100049, China*

Accepted 2016 May 10. Received 2016 May 9; in original form 2016 February 15

ABSTRACT

By cross-matching the currently largest optical catalogue of galaxy clusters and the NVSS radio survey data base, we obtain a large complete sample of brightest cluster galaxies (BCGs) in the redshift range of $0.05 < z \leq 0.45$, which have radio emission and redshift information. We confirm that more powerful radio BCGs tend to be these optically very bright galaxies located in more relaxed clusters. We derived the radio luminosity functions of the largest sample of radio BCGs, and find that the functions depend on the optical luminosity of BCGs and the dynamic state of galaxy clusters. However, the radio luminosity function does not show significant evolution with redshift.

Key words: galaxies: clusters: general – galaxies: luminosity function, mass function.

1 INTRODUCTION

Among many galaxies embedded in hot gas inside a galaxy cluster, the brightest cluster galaxy (BCG) is the most massive and luminous galaxy located near the centre of the cluster (e.g. Wen & Han 2015a). BCGs of galaxy clusters differ from other elliptical galaxies in many aspects because of the unique cluster environments they inhabit and their evolution history (e.g. Rafferty et al. 2006; Ma, McNamara & Nulsen 2013). The nuclei of BCGs host supermassive black holes (e.g. Rafferty et al. 2006), so that BCGs manifest their active nuclei by radio jets that are fed back to intracluster medium (see McNamara & Nulsen 2007). BCGs are more likely to be radio loud than other galaxies (e.g. Burns, White & Hough 1981; Best et al. 2007). The radio emission of BCGs is related to both nuclei activities of BCGs and cluster properties.

Previously there has been much effort to decouple the effect of galaxy properties and cluster environment on radio emission of BCGs. Without the large radio sky survey data, small samples of galaxy clusters, usually less than a hundred, have been observed for statistics in radio band (e.g. Burns et al. 1981; Zhao, Burns & Owen 1989; Burns 1990; Ball, Burns & Loken 1993). The fraction of BCGs being radio loud above a given threshold of radio flux density or luminosity has often been investigated for some cluster samples to examine possible links between BCG radio emission and the cluster cooling flows (e.g. Peres et al. 1998; Mittal et al. 2009) or cluster mass and X-ray luminosity (e.g. Lin & Mohr 2007; Ma et al. 2011; Stott et al. 2012) or dynamic states (e.g. Lin & Mohr 2007; Kale et al. 2015). Mittal et al. (2009) found that BCG radio luminosities are correlated with cluster cooling time, the mass of supermassive black holes and also X-ray luminosity of strong cool-core clusters. Kale et al. (2015) found that a larger fraction of BCGs in relaxed clusters is radio loud than those in merging clusters.

Because of large data scatters, the statistics can be improved using large samples of BCGs observed by radio survey data. von der Linden et al. (2007) and Best et al. (2007) cross-identified 625 BCGs of the C4 cluster sample (Miller et al. 2005) with the radio data of NVSS and FIRST surveys (Becker, White & Helfand 1995; Condon et al. 1998), and found that the fraction of radio-loud BCGs depends on optical luminosity or the stellar mass of BCGs, but not on the cluster velocity dispersion. Antognini, Bird & Martini (2012) got a sample of 151 FR-II type BCGs by looking at the NVSS and FIRST images of the MaxBCG clusters (Koester et al. 2007), and concluded similarly that both jet power and radio-loud fraction are correlated with the *r*-band luminosity of BCGs, but not with the cluster richness. By cross-matching the MaxBCG cluster catalogue (Koester et al. 2007) with the FIRST radio survey data (Becker et al. 1995), Croft, de Vries & Becker (2007) obtained a very large sample of 2615 radio BCGs with $L_{1.4\,\mathrm{GHz}} > 10^{23}$ W Hz^{-1}, and confirmed that the radio-loud fraction depends on the *r*-band absolute magnitude and hence the converted stellar mass of BCGs, from about 5 per cent at $10^{10.7}$ $\mathrm{M}_{\odot}$ to about 30 per cent at $10^{11.6}$ $\mathrm{M}_{\odot}$ and that the fraction is larger for the BCGs in richer clusters. Ma et al. (2013) obtained a large sample of 357 radio BCGs by cross-correlating galaxy clusters in eight X-ray catalogues and NVSS radio sources, and confirmed that the radio fraction increases moderately with redshift and cluster X-ray luminosity. They also found that the radio power is greater in more massive clusters and at higher redshifts, which implies possible redshift evolution of BCG radio emission power. Recently, Hogan et al. (2015) investigated 437 radio BCGs with multifrequency observational images, and found that the core emission is more frequently associated with BCGs with [O III] emission that is the canonical tracer for active galactic nucleus (AGN) activity. See Table 1 for a summary of these previous samples.

★ E-mail: hjl@nao.cas.cn

Table 1. A list of statistical studies of radio BCGs with a sample size over 100.

Authors	Cluster sample	Redshift range	Radio data	Flux limit	No. of radio BCGs
Lin & Mohr (2007)	342 NORAS/REFLEX	$z < 0.2$	NVSS	10 mJy	122
von der Linden et al. (2007)	625 C4 clusters	$0.02 < z < 0.1$	NVSS/FIRST	5 mJy	252
Best et al. (2007)	484 C4 clusters	$0.02 < z < 0.1$	NVSS/FIRST	5 mJy	252
Croft et al. (2007)	13 240 MaxBCG	$0.1 \leq z \leq 0.3$	FIRST		2615
Antognini et al. (2012)	13 823 MaxBCG	$0.1 \leq z \leq 0.3$	FIRST/NVSS	0.75 mJy	151
Ma et al. (2013)	685 X clusters	$0.1 \leq z \leq 0.6$	NVSS	3 mJy	357
Hogan et al. (2015)	720 REFLEX/(e)BCS	$0.03 < z \leq 0.45$	NVSS/SUMSS/ATCA/VLA	15 mJy	437
This work	62 686 WH15	$0.05 < z \leq 0.45$	NVSS/FIRST	5 mJy	7138

More fundamental studies of the BCG radio emission or its difference from other galaxies and their dependence on cluster properties should work on the radio luminosity function that is a measure of the variation of BCG space density with radio luminosity. To construct a good radio luminosity function, a complete sample of objects is needed with known redshifts as well as good measurements of radio emission. Such studies have often been conducted for galaxies and AGNs (e.g. Condon 1989; Donoso, Best & Kauffmann 2009; Best & Heckman 2012; Mao et al. 2012; Simpson et al. 2012; van Velzen et al. 2012; Best et al. 2014). The radio luminosity functions for AGNs and star-forming (SF) galaxies have been found to be very different (e.g. Sadler et al. 2002; Mauch & Sadler 2007) but have no significant evolution with redshift (e.g. McAlpine & Jarvis 2011; Padovani et al. 2011; McAlpine, Jarvis & Bonfield 2013; Padovani et al. 2015; Prescott et al. 2016). The radio luminosity functions for BCGs have been tried based on small samples of radio measurements (e.g. Ball et al. 1993; Lin & Mohr 2007).

In this paper, we cross-match the currently largest optical catalogue of galaxy clusters (Wen & Han 2015b) with the largest radio survey data base of the NVSS and FIRST (Becker et al. 1995; Condon et al. 1998). As shown in Section 2, we can get the largest complete sample of radio BCGs. With such a sample, we study the possible dependence of BCG radio emission on BCG properties and cluster environment in Section 3, and then work on the radio luminosity function of BCGs in Section 4. The conclusions are given in Section 5.

Throughout this paper, we assume a Λ cold dark matter cosmology, taking $H_0 = 100\,h\,\mathrm{kms^{-1}Mpc^{-1}}$, with $h = 0.7$, $\Omega_\mathrm{m} = 0.3$ and $\Omega_\Lambda = 0.7$.

2 BCG SAMPLE AND RADIO EMISSION POWER

Based on the photometric data of the Sloan Digital Sky Survey (SDSS) Data Release 8 (DR8; Aihara et al. 2011), Wen, Han & Liu (2012) identified 132 684 galaxy clusters. Recently, Wen & Han (2015b, hereafter WH15) have updated the parameters of these clusters with spectroscopic redshift data in DR12 (Alam et al. 2015) and further identified 25 419 new clusters. In total there are 158 103 galaxy clusters in the WH15 cluster catalogue. This sample of galaxy clusters is complete up to redshift $z \sim 0.5$ for massive clusters of $M_{500} > 2 \times 10^{14}$ $\mathrm{M}_\odot$ (see fig. 6 in Wen et al. 2012), which was further verified by their redshift distribution in fig. 7 of WH15. Here, we take 62 686 galaxy clusters with a redshift $z \leq 0.45$ and a richness $R_{L*} \geq 12$ in the sky region of 9376 deg^2 of the SDSS-III's Baryon Oscillation Spectroscopic Survey DR12 as the parent sample in the following study. The cluster parameters, such as richness R_{L*} and redshift z (including 56 340 spectroscopic and 6436 photometric redshifts), of these clusters are directly taken from WH15. As shown in WH15, the cluster richness R_{L*} is a good measure of optical mass proxies with a scatter of 0.17 dex. The *r*-band absolute magnitude of BCGs is corrected for redshift evolution by using $M_\mathrm{r}^\mathrm{e} = M_\mathrm{r}^\mathrm{SDSS} + Qz$, with $Q = 1.16$ as done in WH15. The BCG dominance, defined as the difference of absolute magnitudes of the first and second BCGs, $M_{\mathrm{r},2} - M_{\mathrm{r},1}$, can statistically indicate the dynamic state of galaxy clusters (Wen & Han 2013).

To get the radio emission flux densities of these BCGs, we cross-match the optical BCG sample with the NVSS radio source catalogue that is 99 per cent complete above 3.5 mJy (Condon et al. 1998). Our approach is quite similar to those of Best et al. (2005a), and we obtain our radio BCG sample with a few steps. First, the radio flux density limit of 5 mJy is adopted to ensure that two individual components of a BCG above 2.5 mJy are not missed, and we find the NVSS radio sources within a projection distance of 500 kpc from BCGs, which in general is sufficiently large to pick up radio emission components from BCGs. A total of 15 387 BCGs are found to be associated with 18 600 radio sources. Naturally some of these sources come from BCGs, but others are background radio sources or the radio emission from other galaxies instead of BCGs. Among them, 12 885 BCGs have only one NVSS source, and 1985 BCGs have two and 517 BCGs have three or more NVSS sources within the projected 500 kpc.

Secondly, we check the physical association carefully, and adopt a more restricted criterion for the association that is the projection distance of less than 50 kpc. There are 5410 BCGs having one coincident NVSS source within 50 kpc, which are all accepted as radio BCGs; 6526 BCGs having an NVSS source outside 100 kpc from the optical position are directly declined as radio BCGs; 257 of the rest 949 BCGs with one NVSS source between 50 and 100 kpc are accepted as radio BCGs, because either high-resolution FIRST images indicate the physical association or the NVSS source peak is coincident with the optical position of BCG within 50 kpc (see Fig. 1 for example images). For 1985 BCGs with two NVSS sources, we found that 839 BCGs have one NVSS source within 50 kpc, though there is the other source with a very different flux density, which we adopt as radio BCGs with a flux of the coincident source; 28 BCGs are coincident with one of the double sources, which have similar flux densities (within a factor of 2) probably coming from radio lobes or jets of a radio galaxy at the middle position of two sources, and hence are not radio BCGs; 226 BCGs with two NVSS sources outside 50 kpc are adopted as radio BCGs, because the FIRST and/or NVSS images clearly indicate the association of a BCG and double sources. Similarly, for 517 BCGs with three or more NVSS sources in 500 kpc, we adopt 275 as radio BCGs, because one NVSS source is within 50 kpc from a BCG (excluding five BCGs coincident with one of double sources); 91 BCGs with NVSS sources outside 50 kpc are adopted as radio BCGs because the FIRST and/or NVSS image clearly show the association of the

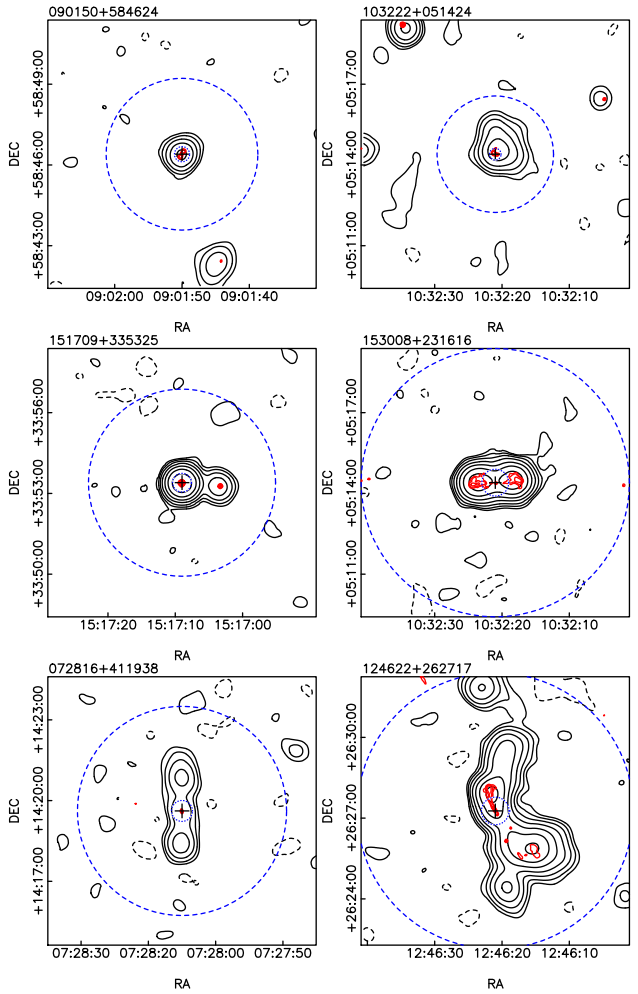

Figure 1. Example images for six radio BCGs. Low-resolution (black) contours are plotted for the NVSS data and high-resolution (red) contours for the FIRST data at levels of $\pm 1, 2, 4, \ldots$ mJy beam^{-1}, with the central cross indicating the optical position of a BCG. The big dashed circle indicates the projection distance of 500 kpc and the small dotted circle near the cross stands for 50 kpc from a BCG. Some radio sources are well coincident with BCGs within 50 kpc, and a small number of double or triple sources have the dominant flux from jets or lobes outside 50 kpc from a BCG.

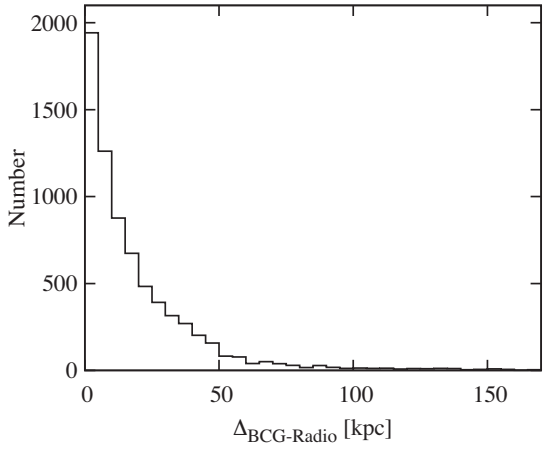

Figure 2. Offsets between optical positions and radio coordinates for 7138 radio BCGs.

BCGs and jets or core. In summary, we identified 7138 radio BCGs in total including 5667 BCGs with one NVSS source, 1105 BCGs with two and 366 BCGs with three or more NVSS sources, see a list in Table 2 for the optical and radio parameters. The offset of radio sources from optical BCG positions are shown in Fig. 2.

We took flux densities of radio sources from the low-resolution survey NVSS images to calculate radio emission power of BCGs. Note that the flux densities of identified multiple radio components of a BCG have to be added together to get $S_{1.4\,\rm GHz}$, and then the radio power is obtained using following function:

$$P_{1.4\,\rm GHz} = 4\pi D_{\rm L}^2 \times S_{1.4\,\rm GHz} \times (1+z)^{1-a}, \quad (1)$$

where $P_{1.4\,\rm GHz}$ is in W Hz^{-1}, $D_{\rm L} = (1+z)\frac{c}{H_0}\int_0^z \frac{{\rm d}z'}{\sqrt{\Omega_{\rm m}(1+z')^3+\Omega_\Lambda}}$ is the luminosity distance of a cluster at a redshift z, $S_{1.4\,\rm GHz}$ is the radio flux at 1.4 GHz from the NVSS and $(1+z)^{(1-a)}$ is the k-correction term with the spectral index a of radio BCGs. We adopt the statistical mean of $a = 0.74$ obtained by Lin & Mohr (2007) for all sources. The radio power distribution of 7138 BCGs is shown in Fig. 3.

Among them, 1594 radio BCGs are from massive clusters of $M_{500} > 2 \times 10^{14}$ M$_\odot$, which form a radio-flux-limited complete sample of BCGs that can be used for deriving the radio luminosity function of BCGs in Section 4. We are confident that the massive

Table 2. The optical and radio parameters for 7138 radio BCGs (see online Supporting Information for the full table).

RA (J2000)	Dec. (J2000)	z	R_{L*} (L^*)	$M_{\rm r}^{\rm e}$ (mag)	$M_{\rm r,2} - M_{\rm r,1}$ (mag)	$S_{1.4\,\rm GHz}$ (mJy)	$P_{1.4\,\rm GHz}$ (10^{24} WHz^{-1})	$\Delta_{\rm BCG-Radio}$ (kpc)
0.203 27	8.666 54	0.4085	31.24	−22.95	0.35	11.8	7.25	11.4
0.203 76	−3.019 15	0.3732	22.17	−22.78	0.66	15.6	7.69	5.7
0.205 52	−0.845 25	0.4110	28.58	−23.18	1.00	24.2	15.09	33.9
0.273 41	34.465 76	0.2474	23.53	−23.09	1.44	37.6	7.00	14.8
0.312 98	−8.446 18	0.3288	17.69	−23.01	0.43	151.1	54.95	19.0
0.325 37	28.995 14	0.4247	43.16	−23.92	1.22	10.9	7.36	5.0
0.423 76	1.980 04	0.4377	29.31	−23.17	0.28	5.5	4.00	69.8
0.477 82	5.665 44	0.2399	14.48	−22.89	1.01	29.3	5.08	42.5
0.534 73	19.290 01	0.1469	12.44	−23.81	0.55	17.6	1.00	37.3
0.545 85	27.828 13	0.3354	27.48	−23.37	1.08	5.4	2.06	16.3
0.566 85	14.856 23	0.2967	13.02	−23.10	0.74	37.6	10.71	114.6
0.574 05	−7.263 82	0.3257	19.03	−23.38	0.88	14.1	5.01	19.3
0.603 04	−0.547 98	0.2902	27.76	−23.04	0.18	19.0	5.14	24.4
0.676 32	−0.222 17	0.2989	26.52	−23.36	0.82	40.8	11.83	20.5
0.686 71	−1.821 53	0.3941	17.68	−23.05	0.84	14.2	7.99	6.9

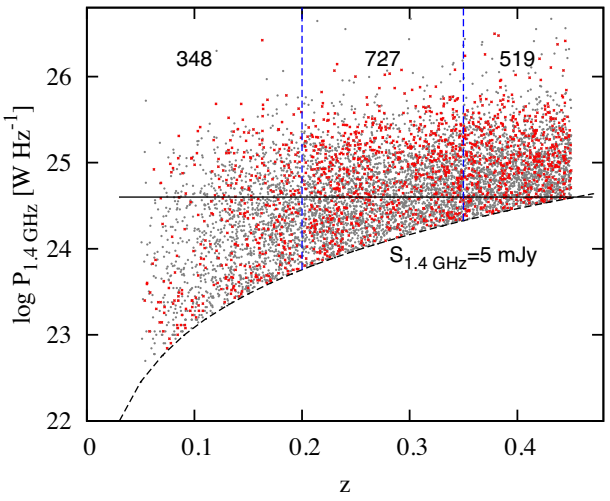

Figure 3. Radio emission power of 7138 BCGs. All BCGs have a radio flux density $S_{1.4\,\mathrm{GHz}} > 5$ mJy. BCGs of a complete sample of 1594 massive clusters of $M_{500} > 2 \times 10^{14}$ $M_{\odot}$ (equivalent to $R_{L*} > 35$) are indicated by (red) crosses. Sub-samples for three redshift ranges are divided by vertical dashed lines that will be used for checking the redshift evolution of the BCG radio luminosity function in Section 4. Above a black line of $\log P_{1.4\,\mathrm{GHz}} = 24.6$ is a power-limited complete sample of radio BCGs up to $z = 0.45$.

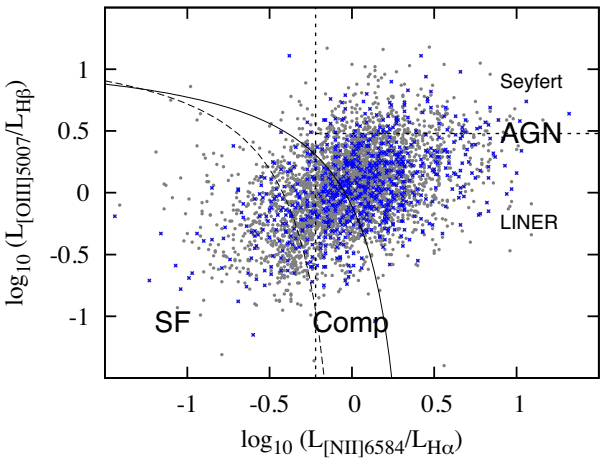

Figure 4. The BPT diagram of emission-line ratios for 2763 BCGs that have a spectrum with a median signal-to-noise ratio greater than 10. Among them, 619 BCGs have their radio emission detected with $S_{1.4\,\mathrm{GHz}} > 5$ mJy, as indicated by little (blue) crosses. The solid curve is the demarcation for defining SF galaxies (Kewley et al. 2001), and the dashed curve is the demarcation for classifying AGNs (Kauffmann et al. 2003). Dotted lines on $L_{[\mathrm{O\,III}]5007}/L_{\mathrm{H}\beta} = 3$ and $L_{[\mathrm{N\,II}]6584}/L_{\mathrm{H}\alpha} = 0.6$ are used for dividing low-ionization nuclear emission-line regions and Seyferts.

cluster sample is nearly 100 per cent complete during the cluster identification (Wen et al. 2012), and the detection of radio emission for $S_{1.4\,\mathrm{GHz}} > 5$ mJy is at least 95 per cent complete in the low-resolution NVSS survey even when BCGs have two components. On the other hand, the radio detection of BCGs is power-limited complete above a threshold of $\log P_{1.4\,\mathrm{GHz}} > 24.6$ up to $z = 0.45$.

3 FRACTION OF RADIO BCGS AND DEPENDENCE ON BCG AND CLUSTER PROPERTIES

As shown above, only 7138 BCGs (11.4 per cent) of 62 686 galaxy clusters of $z < 0.45$ have radio emission with a flux density of $S_{1.4\,\mathrm{GHz}} > 5$ mJy. No doubt that more BCGs can be detected in radio by more sensitive observations. In this section, we check the possible dependence of the radio fraction on BCG characteristics and cluster properties.

3.1 Radio fraction of spectroscopically classified BCGs

Most BCGs are elliptical galaxies with active nuclei, showing AGN properties. Nevertheless, a few per cent of galaxy clusters show a cooling flow near the centre of clusters (see Fabian 1994; Allen, Evrard & Mantz 2011), which is probably related to the on-going or post-star formation features of BCGs (e.g. O'Dea et al. 2010; Liu et al. 2012a; Liu, Mao & Meng 2012b). It is intriguing to know how many BCGs have AGNs and how many of them possess star-formation features.

In general, galaxies can be broadly classified as SF galaxies, radio-loud AGNs and composites (e.g. Machalski & Godlowski 2000; Sadler et al. 2002; Best et al. 2005a; Mauch & Sadler 2007) according to spectra of galaxies or their nuclei. The BPT (Baldwin, Phillips & Terlevich 1981) diagram of line ratios has been used widely as a diagnostic to separate radio-loud AGNs from SF galaxies (e.g. Kauffmann et al. 2003; Best et al. 2007; Best & Heckman 2012). In our parent sample of 62 686 galaxy clusters, 56 340 BCGs have already observed spectra. However, to get the line ratios among Hα, Hβ, [OIII]5007 and [NII]6584, the spectra of BCGs should have a good signal-to-noise ratio. From the value-added spectroscopic catalogues[1] produced by a research group from the Max Planck Institute for Astrophysics and the Johns Hopkins University (see Brinchmann et al. 2004; Tremonti et al. 2004), 2763 BCGs have a spectrum with a median signal-to-noise ratio per pixel of the whole spectrum $sn_{\mathrm{median}} > 10$ and with the pipeline warning flags $zWarning = 0$, from which four spectral lines of Hα, Hβ, [O III]5007 and [N II]6584 are significantly detected. The BPT diagram of 2763 BCGs is plotted in Fig. 4. According to the demarcation for defining SF galaxies and AGNs (Kewley et al. 2001; Kauffmann et al. 2003), 1303 BCGs (47.2 per cent of 2763) have an AGN, 357 BCGs (12.9 per cent) have SF features and the rest 1103 BCGs are composite galaxies. Among all these BCGs, 619 (22.4 per cent of 2763) BCGs have radio emission detected above $S_{1.4\,\mathrm{GHz}} = 5$ mJy, as indicated in Fig. 4.

The BCGs with the four emission lines consists of bright nearby (majority $z < 0.2$) BCGs, but do not form a complete sample by any means. Nevertheless, the statistics on the radio fraction of these BCGs is given in Table 3 and the BPT diagram in Fig. 4 shows that not all radio BCGs possess AGNs, and that 10.8 per cent (i.e. 67/619) radio BCGs are SF galaxies, not necessary just elliptical galaxies. The AGN percentage is larger for radio BCGs (i.e. 63.2 per cent = 391/619) than for BCGs in general (i.e. 47.2 per cent = 1303/2763).

3.2 Radio power versus optical characteristics of BCGs

The BCGs are unusual galaxies. By using the large sample of 7138 radio BCGs, we here investigate the possible dependence of BCG

[1] http://wwwmpa.mpa-garching.mpg.de/SDSS/DR7/

Table 3. Radio fraction of spectroscopically classified BCGs.

BCG samples	SF	Comp	AGN	Sum
BCGs with four lines detected	357	1103	1303	2763
No. of Radio BCGs	67	161	391	619
Radio fraction	18.8 per cent	14.6 per cent	30.0 per cent	22.4 per cent
BCG no. of $\log P_{1.4\,\mathrm{GHz}} > 24.6$	25	57	151	233
Radio fraction	7.0 per cent	5.2 per cent	11.6 per cent	8.4 per cent

radio power on the absolute magnitude, velocity dispersion and luminosity of [O III]5007 line. The absolute *r*-band magnitude is an indicator of stellar mass of galaxies and is also related to the mass of a central black hole (e.g. see equations 8–10 in Mittal et al. 2009). The stellar velocity dispersion has been well-established to relate to the mass of central black hole (Tremaine et al. 2002; Marconi & Hunt 2003). Since the high-ionization [O III] forbidden line is emitted by a filamentary gas related to jets (McCarthy 1993), it is the indicator of AGN activity (e.g. Maiolino & Rieke 1995). Besides the evolution-corrected *r*-band absolute magnitude of 7138 radio BCGs, we obtain the stellar velocity dispersion σ of 2884 BCGs and the luminosity of [O III]5007 line of 1237 BCGs from the value-added spectroscopic catalogues produced by a research group from the Max Planck Institute for Astrophysics and the Johns Hopkins University (see Brinchmann et al. 2004; Tremonti et al. 2004).

As shown in the top panels of Fig. 5, the radio power data in all three panels are rather scattered against the absolute magnitude, the velocity dispersion and [O III]5007 line luminosity of BCGs. Our results are consistent with the plots previously obtained for a small sample of BCGs by Mittal et al. (2009) and large samples of BCGs by Croft et al. (2007), Antognini et al. (2012) and Hogan et al. (2015). The mild or strong correlation between radio power and the absolute magnitude found for radio galaxies (e.g. Calvani, Fasano & Franceschini 1989) is not shown for radio BCGs, even for the complete sample of radio BCGs in massive clusters. No significant correlation between the radio power and stellar velocity dispersion is found for BCGs. The Spearman rank–order correlation coefficient *r* (see p. 34 of Press et al. 1992) in each panel explains the strength of the correlation. Nevertheless, a weak correlation ($r' = 0.41$) exists between the radio power and luminosity of [O III] line of BCGs, shown in the top-right panel of Fig. 5, though not as strong as radio galaxies (Saunders et al. 1989; McCarthy 1993; Willott et al. 1999; Sikora et al. 2013). Very probably line emission is fundamentally related with core radio emission (Hogan et al. 2015) of high-excitation radio galaxies (Best & Heckman 2012). The radio power of BCGs in this paper includes all radio emission components, not just limited to core.

Note that the fraction of radio loudness of BCGs has been related to the absolute magnitude or stellar mass (Best et al. 2007; Mittal et al. 2009; Kale et al. 2015). We will check it together with cluster richness in Section 3.4, but we show the probability distribution of two power-limited complete samples of radio BCGs along the absolute magnitude in the left-hand panel of Fig. 6. The Kolmogorov-Smirnov test (see p. 617 of Press et al. 1992) shows that the BCG samples of $24.6 < \log P_{1.4\,\mathrm{GHz}} < 25.0$ and of $\log P_{1.4\,\mathrm{GHz}} > 25.0$ have different distributions of the absolute magnitude or stellar mass with an obvious shift of more powerful radio BCGs to optical brighter magnitude, which echoes with the previous conclusion (e.g. Best et al. 2007; von der Linden et al. 2007; Antognini et al. 2012; Hogan et al. 2015) that the radio-loud fraction is larger for more massive BCGs for a given flux density threshold.

3.3 Radio power of BCGs versus cluster properties

We investigate here the possible correlation between the radio power of BCGs and cluster environments. Most of the previous studies have worked on the X-ray cluster samples (e.g. Lin & Mohr 2007; Ma et al. 2013; Hogan et al. 2015) and checked if the BCG radio emission or the fraction of radio BCGs depends on cluster dynamic state or cluster mass. Observations of small sample of clusters show that BCGs in relaxed clusters have higher possibility to be radio loud than those in unrelaxed clusters, and that radio power of BCGs seems to correlate with dynamical parameters of clusters (e.g. Peres et al. 1998; Mittal et al. 2009; Kale et al. 2015). Here we work on the optical cluster sample.

Two classes of cluster parameters are investigated for their relation with BCG radio emission power. First is on cluster mass. Mass of galaxy clusters is in general estimated from the X-ray data (e.g. Reiprich & Böhringer 2002). Up to now, only a few thousand galaxy clusters have their mass so estimated (e.g. Vikhlinin et al. 2009; Mantz et al. 2010; Piffaretti et al. 2011). We get X-ray-estimated mass for 198 host clusters with radio BCGs from the compiled catalogue by WH15 and the mass estimated via Sunyaev–Zel'dovich (SZ) effect for 90 clusters from the recent Planck cluster catalogue (Planck Collaboration XXVII 2015). The cluster richness, R_{L*}, derived from the total optical luminosity of member galaxies is used as an optical mass proxy of clusters as verified by WH15. In the middle rank of Fig. 5, the BCG radio power is plotted against R_{L*} and the cluster mass is estimated from X-ray and SZ observations. Data are scattered, but show weak correlations in all three panels, which indicates the tendency that more powerful radio BCGs are hosted by more massive clusters. The BCGs in clusters with smaller richnesses or less masses have a distribution of radio power peaked at a smaller power than those in richer clusters, which is consistent with the results of Lin & Mohr (2007) and Ma et al. (2013). This is understandable, because BCGs are brighter in richer clusters (Wen et al. 2012), which could produce a bit stronger radio emission (see discussion above). It is intriguing, however, to see that there is no correlation between the radio power and cluster richness for the radio BCGs of a complete sample of massive clusters (the left-hand panel of middle rank of Fig. 5), and no difference is found for the cluster richness distributions of two radio power-limited complete sub-samples of BCGs (see the middle panel of Fig. 6). Such a result implies for no dependence of BCG radio emission on cluster richness (Antognini et al. 2012). Notice that these two complete sub-samples of BCGs are hosted by clusters with only a small range of richness and that the correlation is shown between radio power and M_{SZ}. Therefore, whether there is any dependence of BCG radio power on richness or cluster mass has to be concluded by further investigations of a large cluster sample with a much large range of mass or richness.

Next class of cluster parameters is on dynamical states of galaxy clusters. In principle, the three-dimensional mass and velocity distributions of gas and member galaxies should be measured to

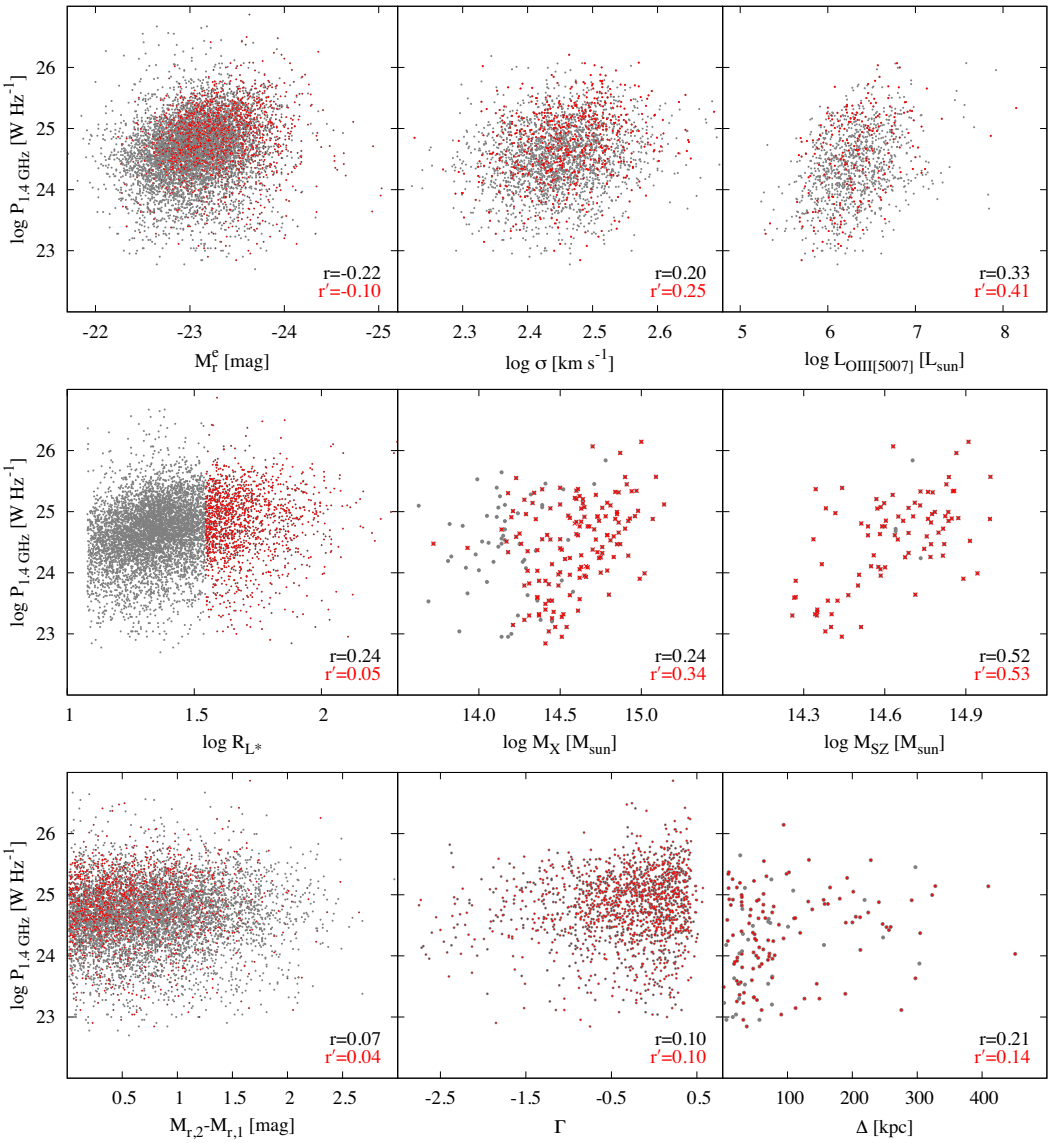

Figure 5. Radio power of BCGs are plotted against BCG optical parameters in top panels (the left for the evolution-corrected r-band absolute magnitude M_r^e, the middle for stellar velocity dispersion σ and the right for the luminosity of [O III] lines $L_{[O\,III]}$), cluster properties in middle-rank panels (the left for richness R_{L*}, the middle for X-ray-estimated mass M_X and the right for SZ-estimated mass M_{SZ}) and cluster dynamic states in bottom panels (the left for BCG dominance $M_{r,2} - M_{r,1}$, the middle for optical dynamical parameter Γ from Wen & Han (2013) and the right for the offset Δ of X-ray peak from BCG), if these parameters are available (see the text). The radio BCGs in a complete sample of massive clusters of $M_{500} > 2 \times 10^{14}$ $M_\odot$ are indicated by (little red) crosses. The Spearman correlation coefficients are given in the bottom-right corner of each panel for both all radio BCGs (r) and the radio-flux-limited complete sample (r').

describe if a galaxy cluster is dynamically relaxed or in a state of merging or dynamically disturbed. In practice, one-dimensional measurements of velocity distribution of member galaxies (e.g. Dressler & Shectman 1988) and the two-dimensional distribution of hot gas (e.g. Mann & Ebeling 2012) or member galaxies (e.g. Wen & Han 2013) have been quantitatively analysed for cluster dynamic states. We here get dynamical parameters Γ of 1594 clusters from Wen & Han (2013) and from new calculations, and the offsets of BCGs from the peak of X-ray images for 149 host clusters from Piffaretti et al. (2011). We noticed that the BCG dominance $M_{r,2} - M_{r,1}$ can statistically be used as being an indicator of dynamical parameter for galaxy clusters (see Wen & Han 2013). These dynamical parameters are not significantly correlated with radio power of BCGs, as shown in the lower panels of Fig. 5. However, the distributions of optical dynamical parameters Γ are slightly different for the two radio-power-limited complete samples of BCGs in massive clusters, as shown in the right-hand panel of Fig. 6. Slightly more radio-powerful BCGs are detected in more dynamically relaxed clusters, which is consistent with the results of Kale et al. (2015).

3.4 Fraction of radio-loud BCGs versus BCG magnitude and cluster richness

Because of large data scatter, it is very hard to correlate the radio power with BCG properties and cluster environments as shown above. The fraction of radio loudness, f_{RL}, defined as the percentage or the ratio between the radio detected objects and the full sample,

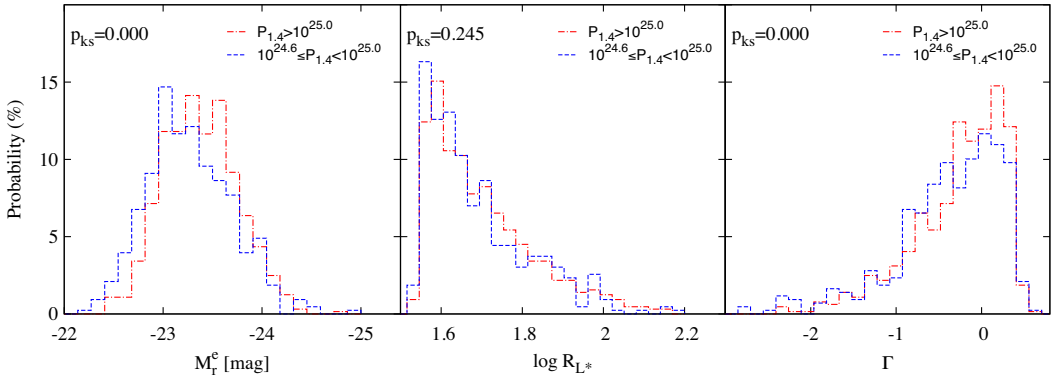

Figure 6. The probability distributions for two power-limited complete sub-samples of a massive cluster sample of $M_{500} > 2 \times 10^{14}$ $M_{\odot}$ along the evolution corrected r-band absolute magnitude M_r^e (the left), cluster richness R_{L*} (the middle) and the cluster dynamic state parameter Γ (the right). The KS-test probability for the two sub-samples is given in the upper-left corner of each panel.

has been used to check the possible dependence of radio emission on other galaxy properties (e.g. Best et al. 2005b). The fraction of radio BCGs has been related to either the absolute magnitude of BCGs (e.g. Best et al. 2007; Croft et al. 2007; von der Linden et al. 2007; Antognini et al. 2012) or the X-ray luminosity and richness of galaxy clusters (e.g. Ma et al. 2013), but not both yet. Here, we take this large sample of radio BCGs to study the dependence of radio-loud fraction in two dimensions on both BCG and cluster properties.

Remember that 7138 radio-loud BCGs were identified from a parent sample of 62 686 optical clusters using the NVSS and FIRST survey data with a total flux density threshold of $S_{1.4\,\mathrm{GHz}} > 5$ mJy, and 4208 of which are above the radio power threshold of $P_{1.4\,\mathrm{GHz}} = 10^{24.6}$ WHz^{-1} in the redshift range $0.05 < z \leq 0.45$ (see Fig. 3). We define the radio-loud fraction f_{RL} (M_r^e, R_{L*}) as the number ratio of these radio BCGs to the BCG numbers of the parent cluster sample for a given small range of the BCG magnitude and cluster richness. The radio fraction is then checked in two dimensions for its possible dependence on the BCG luminosity and cluster richness. As shown in Fig. 7, for both power-limited radio BCG sample and the flux-limited radio BCG sample, there is a very clear tendency that the radio fraction increases with both BCG magnitude and cluster richness, from ∼1 per cent in the lower-left corner to ∼20 per cent in the top-right corner, that is for very bright BCGs in massive rich clusters. To disentangle their effects, the dependence of radio fraction on one parameter should be checked in Fig. 7 only in a small range of the other parameter. Integrating data in Fig. 7 over one dimension gives a global dependence of the radio fraction on the other dimension, echoing the results previously obtained by Croft et al. (2007), von der Linden et al. (2007), Best et al. (2007), Antognini et al. (2012) and Ma et al. (2013).

We conclude that the BCG mass and cluster environments only statistically affect the BCG radio emission, but not through individual cases.

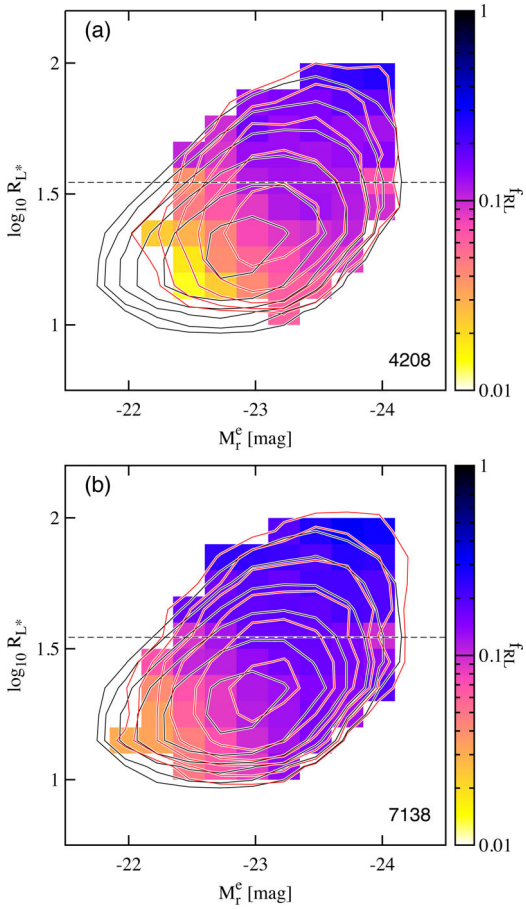

Figure 7. The fraction of radio-loud BCGs, f_{RL}, varies with the r-band absolute magnitude of BCG and cluster richness. The upper panel is calculated by using 4208 radio BCGs with a power-limited threshold of $P_{1.4\,\mathrm{GHz}} > 10^{24.6}$ WHz^{-1}, and the lower panel using 7138 radio BCGs with a flux limit of $S_{1.4\,\mathrm{GHz}} > 5$ mJy, both of which are compared with 62 686 BCGs in the optical parent cluster sample. Above the dash line of $R_{L*} = 35$ is a complete BCG sample of massive clusters of $z < 0.45$. A pixel is shown only if there are more than 10 radio BCGs. Overlaid are red contours for the number distribution of radio BCGs at levels of 5×2^n ($n = 0, 1, 2, 3, 4, 5$) per pixel, and black contours for 62 686 BCGs of the parent sample at levels of $5 \times 2^n \times D$ ($n = 0, 1, 2, 3, 4, 5$), and $D = 62\,686/4208$ or $62\,686/7138$ for the two samples, respectively.

4 RADIO LUMINOSITY FUNCTION OF BCGS

We noticed that the fraction of radio BCGs depends on the threshold of radio observation. The radio power data are very scattered against BCG and cluster properties. Luminosity function is an important tool to study the evolution of space population. We now work on radio luminosity function of BCGs, and check the dependence of the function on the BCG and cluster properties.

Table 4. Radio luminosity functions at 1.4 GHz for radio-loud BCGs in three redshift ranges (only for more than five objects each bin).

	$0.05 < z \leq 0.20$		$0.20 < z \leq 0.35$		$0.35 < z \leq 0.45$	
$\log P_{1.4\,\mathrm{GHz}}$ ($\mathrm{WHz^{-1}}$)	N	$\log\Phi$ ($\mathrm{Mpc^{-3}dex^{-1}}$)	N	$\log\Phi$ ($\mathrm{Mpc^{-3}dex^{-1}}$)	N	$\log\Phi$ ($\mathrm{Mpc^{-3}dex^{-1}}$)
23.1	10	$-7.39^{+0.12}_{-0.17}$				
23.3	22	$-7.34^{+0.08}_{-0.10}$				
23.5	22	$-7.62^{+0.08}_{-0.10}$				
23.7	39	$-7.63^{+0.07}_{-0.08}$				
23.9	28	$-7.85^{+0.08}_{-0.09}$	21	$-7.69^{+0.09}_{-0.11}$		
24.1	33	$-7.78^{+0.07}_{-0.08}$	34	$-7.98^{+0.07}_{-0.08}$		
24.3	26	$-7.88^{+0.08}_{-0.10}$	92	$-7.88^{+0.04}_{-0.05}$		
24.5	38	$-7.72^{+0.07}_{-0.08}$	86	$-7.95^{+0.04}_{-0.05}$	61	$-7.95^{+0.05}_{-0.06}$
24.7	31	$-7.81^{+0.07}_{-0.09}$	93	$-7.91^{+0.04}_{-0.05}$	77	$-8.08^{+0.05}_{-0.05}$
24.9	32	$-7.79^{+0.07}_{-0.08}$	105	$-7.86^{+0.04}_{-0.04}$	92	$-8.00^{+0.04}_{-0.05}$
25.1	28	$-7.85^{+0.08}_{-0.10}$	117	$-7.81^{+0.04}_{-0.04}$	100	$-7.97^{+0.04}_{-0.05}$
25.3	21	$-7.97^{+0.09}_{-0.11}$	87	$-7.94^{+0.04}_{-0.05}$	82	$-8.05^{+0.05}_{-0.05}$
25.5	7	$-8.45^{+0.14}_{-0.21}$	55	$-8.14^{+0.06}_{-0.06}$	60	$-8.19^{+0.05}_{-0.06}$
25.7	7	$-8.45^{+0.14}_{-0.21}$	21	$-8.56^{+0.09}_{-0.11}$	27	$-8.54^{+0.08}_{-0.09}$
25.9			8	$-8.98^{+0.13}_{-0.19}$	6	$-9.19^{+0.15}_{-0.23}$
26.1			6	$-9.10^{+0.15}_{-0.23}$		
Total	348		727		519	

The luminosity function $\Phi(P)$ stands for the comoving space density of a kind of objects in a complete sample for a given luminosity P (e.g. Auriemma et al. 1977; Condon 1989). Considering the possible cosmological evolution, the global average space density should be calculated at the present epoch for the *local* luminosity function (e.g. Condon 1989; Mauch & Sadler 2007). As shown in Section 2, we have got a complete sample of massive clusters of $M_{500} > 2 \times 10^{14}\,\mathrm{M_\odot}$ (i.e. $R_{L*} > 35$) within the redshift range of $0.05 < z \leq 0.45$, from which 1594 BCGs have been detected in radio surveys above the flux limit of $S_{1.4\,\mathrm{GHz}} > 5\mathrm{mJy}$ (see the crosses in Fig. 3). This forms a complete radio BCG sample for radio luminosity function of BCGs.

The radio luminosity functions $\Phi(P)$ are calculated in the standard way, as $\Phi(P) = \sum_i 1/V_i$. Here, V_i is the volume in which the ith BCG with a radio power between P and $P + \mathrm{d}P$ could be detected (Schmidt 1968; Condon 1989; Best & Heckman 2012). For N sources of a complete sample detected in the redshift range of $z_{\min} < z_i < z_{\max}$, in a given sky region, all of them have $V_i = V_{z_{\max}} - V_{z_{\min}}$, so that $\Phi(P) = \sum_{i=1}^{N} 1/V_i = N/(V_{z_{\max}} - V_{z_{\min}})$. Note here that the sky area of 9376 $\mathrm{deg^2}$ (i.e. 2.85 sr) for the complete sample of massive clusters and hence the radio BCGs have to be taken into account for the calculation of V_i. To study if the radio luminosity functions of BCGs evolve with redshift, we divide the complete sample into three sub-samples with redshift ranges of $0.05 < z \leq 0.20$, $0.20 < z \leq 0.35$ and $0.35 < z \leq 0.45$. Their radio luminosity functions are listed in Table 4 and plotted in Fig. 8. The uncertainties of $\Phi(P)$ here include only the statistical Poissonian errors, and hence are underestimated for some bins with small number of objects.

As shown clearly in Fig. 8, no evolution with redshift can be found from radio luminosity functions obtained from the sub-samples of three different redshift ranges, which is consistent with previous results for radio galaxies (e.g. Sadler et al. 2007; Donoso et al. 2009; McAlpine & Jarvis 2011; Simpson et al. 2012). Following Mauch & Sadler (2007), we fit the radio luminosity functions of three sub-samples together with a two power-law analogous:

$$\Phi(P_{1.4\,\mathrm{GHz}}) = \frac{C_0}{(P_{1.4\,\mathrm{GHz}}/P_0)^{\alpha} + (P_{1.4\,\mathrm{GHz}}/P_0)^{\beta}}, \quad (2)$$

and obtained the best-fitted parameters as

$$C_0 = (9.4 \pm 1.4) \times 10^{-9}\,\mathrm{Mpc^{-3}dex^{-1}};$$

$$P_0 = (39.9 \pm 5.5) \times 10^{24}\,\mathrm{WHz^{-1}};$$

$$\alpha = 3.43 \pm 0.79;$$

$$\beta = 0.12 \pm 0.06.$$

Comparing with the radio luminosity functions of SF galaxies and AGNs obtained by Mauch & Sadler (2007) and Best & Heckman

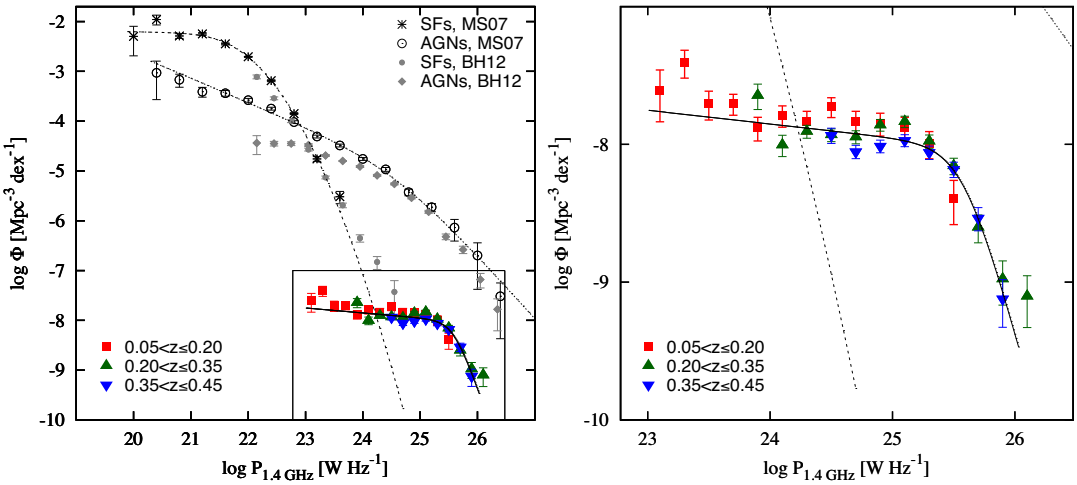

Figure 8. Radio luminosity functions of BCGs derived for sub-samples in three redshift ranges, compared with radio luminosity functions of SF galaxies and AGNs obtained by Mauch & Sadler (2007) and Best & Heckman (2012). The solid line is the best fitting to radio luminosity functions of all BCGs, and dashed and dotted lines stand for the fitting to the function for AGNs and SF in Mauch & Sadler (2007). An enlarged part for radio luminosity functions of BCGs is shown in the right panel.

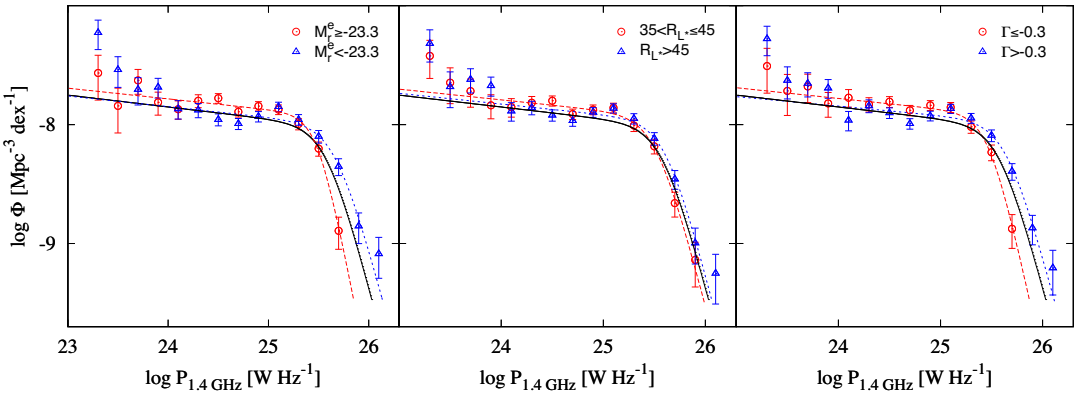

Figure 9. Radio luminosity functions of BCGs in two sub-samples with different ranges of BCG luminosity (the left), cluster richness (the middle) and dynamic states (the right). The black solid lines are the best fitting for all radio BCGs, the same as that in Fig. 8, and dashed and dotted lines are best fittings for two sub-samples. For better comparison, the radio luminosity functions of BCGs in two sub-samples have been rescaled to that of the full sample of BCGs according to source numbers.

Table 5. Fitting parameters of radio luminosity functions of BCG samples.

BCG Sample	C_0	P_0	α	β
All	9.4 ± 1.4	39.9 ± 5.5	3.43 ± 0.79	0.12 ± 0.06
$M_r^e \geq -23.3$	6.3 ± 0.6	32.4 ± 2.4	4.46 ± 0.81	0.08 ± 0.04
$M_r^e < -23.3$	4.5 ± 1.1	50.9 ± 11.1	3.37 ± 1.24	0.14 ± 0.08
$35 < R_{L*} \leq 45$	5.8 ± 0.8	33.6 ± 3.8	3.59 ± 0.67	0.09 ± 0.05
$R_{L*} > 45$	5.1 ± 1.0	44.9 ± 7.8	3.48 ± 0.97	0.13 ± 0.07
$\Gamma \leq -0.3$	5.5 ± 0.7	30.5 ± 3.1	3.75 ± 0.77	0.08 ± 0.05
$\Gamma > -0.3$	5.6 ± 1.1	47.2 ± 8.4	3.40 ± 1.00	0.12 ± 0.07

Notes. C_0 in 10^{-9} Mpc^{-3} dex^{-1}, P_0 in 10^{24} W Hz^{-1}.

(2012), we find that the space density of radio BCGs is significantly lower than AGNs when $P_{1.4\,GHz} \gtrsim 10^{24.5}$ WHz^{-1} or lower than SF galaxies when $P_{1.4\,GHz} \leq 10^{24.5}$ WHz^{-1}. The slope and the tuning points are very different from those of radio luminosity functions of AGNs and SF galaxies.

To check the dependence of radio luminosity functions on the BCG and cluster properties, we divide the 1594 radio BCGs into two half sub-samples according to the BCG absolute magnitude, cluster richness and also dynamical parameter of clusters. The radio luminosity functions of every two sub-samples are shown in Fig. 9 and the best-fitting parameters are listed in Table 5. The functions are normalized according to BCG numbers for easy comparison. We do see different radio luminosity functions for BCGs of different ranges of absolute magnitude or different dynamical states. However, no significant difference can be found for the two BCG samples of slightly different richness ranges. The results imply that more radio power BCGs are associated with optically bright BCGs in the relaxed clusters, confirming the result in Section 3.4 and conclusions by Mittal et al. (2009) and Kale et al. (2015).

5 SUMMARY AND CONCLUSIONS

Based on the largest optical catalogue of galaxy clusters of WH15 and the largest radio survey data base of the NVSS and FIRST, we identified a large sample of 7138 radio-loud BCGs. More than half of radio BCGs host a AGN, and some of them show star-formation features.

We found that the radio power data of BCGs are rather scattered when they are plotted against the BCG absolute magnitudes and cluster mass proxies or cluster dynamical parameters. Very weak or no significant correlations can be found between the radio power and the BCG or cluster parameters. The fraction of radio-loud BCGs has been checked against the BCG absolute magnitudes and cluster richness, and we confirm that the radio-loud fraction of BCGs does increase with BCG luminosity and cluster richness in two dimensions. By using the currently largest complete BCG sample, we construct the radio luminosity functions of BCGs, and do not find any redshift evolution in the redshift range of $0.05 < z \leq 0.45$. Radio luminosity functions are different for BCGs with different ranges of BCG luminosity and the cluster dynamical parameter. We conclude that BCGs are probably more radio powerful if they have a larger absolute magnitude and reside in more relaxed clusters.

ACKNOWLEDGEMENTS

The authors are supported by the National Natural Science Foundation (No. 11473034) and by the Strategic Priority Research Programme 'The Emergence of Cosmological Structures' of the Chinese Academy of Sciences, Grant No. XDB09010200. Funding for SDSS-III has been provided by the Alfred P. Sloan Foundation, the Participating Institutions, the National Science Foundation, and the US Department of Energy. The SDSS-III web site is http://www.sdss3.org/.

REFERENCES

Aihara H. et al., 2011, ApJS, 193, 29
Alam S. et al., 2015, ApJS, 219, 12
Allen S. W., Evrard A. E., Mantz A. B., 2011, ARA&A, 49, 409
Antognini J., Bird J., Martini P., 2012, ApJ, 756, 116
Auriemma C., Perola G. C., Ekers R. D., Fanti R., Lari C., Jaffe W. J., Ulrich M. H., 1977, A&A, 57, 41
Baldwin J. A., Phillips M. M., Terlevich R., 1981, PASP, 93, 5
Ball R., Burns J. O., Loken C., 1993, AJ, 105, 53
Becker R. H., White R. L., Helfand D. J., 1995, ApJ, 450, 559
Best P. N., Heckman T. M., 2012, MNRAS, 421, 1569
Best P. N., Kauffmann G., Heckman T. M., Ivezić Ž., 2005a, MNRAS, 362, 9
Best P. N., Kauffmann G., Heckman T. M., Brinchmann J., Charlot S., Ivezić Ž., White S. D. M., 2005b, MNRAS, 362, 25
Best P. N., von der Linden A., Kauffmann G., Heckman T. M., Kaiser C. R., 2007, MNRAS, 379, 894
Best P. N., Ker L. M., Simpson C., Rigby E. E., Sabater J., 2014, MNRAS, 445, 955

Brinchmann J., Charlot S., White S. D. M., Tremonti C., Kauffmann G., Heckman T., Brinkmann J., 2004, MNRAS, 351, 1151
Burns J. O., 1990, AJ, 99, 14
Burns J. O., White R. A., Hough D. H., 1981, AJ, 86, 1
Calvani M., Fasano G., Franceschini A., 1989, AJ, 97, 1319
Condon J. J., 1989, ApJ, 338, 13
Condon J. J., Cotton W. D., Greisen E. W., Yin Q. F., Perley R. A., Taylor G. B., Broderick J. J., 1998, AJ, 115, 1693
Croft S., de Vries W., Becker R. H., 2007, ApJ, 667, L13
Donoso E., Best P. N., Kauffmann G., 2009, MNRAS, 392, 617
Dressler A., Shectman S. A., 1988, AJ, 95, 985
Fabian A. C., 1994, ARA&A, 32, 277
Hogan M. T. et al., 2015, MNRAS, 453, 1201
Kale R., Venturi T., Cassano R., Giacintucci S., Bardelli S., Dallacasa D., Zucca E., 2015, A&A, 581, A23
Kauffmann G. et al., 2003, MNRAS, 346, 1055
Kewley L. J., Dopita M. A., Sutherland R. S., Heisler C. A., Trevena J., 2001, ApJ, 556, 121
Koester B. P. et al., 2007, ApJ, 660, 239
Lin Y.-T., Mohr J. J., 2007, ApJS, 170, 71
Liu F., Wen Z., Han J., Meng X., 2012a, Sci. China Phys. Mech. Astron., 55, 354
Liu F. S., Mao S., Meng X. M., 2012b, MNRAS, 423, 422
Ma C.-J., McNamara B. R., Nulsen P. E. J., Schaffer R., Vikhlinin A., 2011, ApJ, 740, 51
Ma C.-J., McNamara B. R., Nulsen P. E. J., 2013, ApJ, 763, 63
McAlpine K., Jarvis M. J., 2011, MNRAS, 413, 1054
McAlpine K., Jarvis M. J., Bonfield D. G., 2013, MNRAS, 436, 1084
McCarthy P. J., 1993, ARA&A, 31, 639
Machalski J., Godlowski W., 2000, A&A, 360, 463
McNamara B. R., Nulsen P. E. J., 2007, ARA&A, 45, 117
Maiolino R., Rieke G. H., 1995, ApJ, 454, 95
Mann A. W., Ebeling H., 2012, MNRAS, 420, 2120
Mantz A., Allen S. W., Ebeling H., Rapetti D., Drlica-Wagner A., 2010, MNRAS, 406, 1773
Mao M. Y. et al., 2012, MNRAS, 426, 3334
Marconi A., Hunt L. K., 2003, ApJ, 589, L21
Mauch T., Sadler E. M., 2007, MNRAS, 375, 931
Miller C. J. et al., 2005, AJ, 130, 968
Mittal R., Hudson D. S., Reiprich T. H., Clarke T., 2009, A&A, 501, 835
O'Dea K. P. et al., 2010, ApJ, 719, 1619
Padovani P., Miller N., Kellermann K. I., Mainieri V., Rosati P., Tozzi P., 2011, ApJ, 740, 20
Padovani P., Bonzini M., Kellermann K. I., Miller N., Mainieri V., Tozzi P., 2015, MNRAS, 452, 1263
Peres C. B., Fabian A. C., Edge A. C., Allen S. W., Johnstone R. M., White D. A., 1998, MNRAS, 298, 416
Piffaretti R., Arnaud M., Pratt G. W., Pointecouteau E., Melin J.-B., 2011, A&A, 534, A109
Planck Collaboration XXVII, 2015, preprint (arXiv:1502.01598)
Prescott M. et al., 2016, MNRAS, 457, 730
Press W. H., Teukolsky S. A., Vetterling W. T., Flannery B. P., 1992, Numerical recipes in FORTRAN. The art of scientific computing, 2nd edn. Cambridge Univ. Press, Cambridge
Rafferty D. A., McNamara B. R., Nulsen P. E. J., Wise M. W., 2006, ApJ, 652, 216
Reiprich T. H., Böhringer H., 2002, ApJ, 567, 716
Sadler E. M. et al., 2002, MNRAS, 329, 227
Sadler E. M. et al., 2007, MNRAS, 381, 211
Saunders R., Baldwin J. E., Rawlings S., Warner P. J., Miller L., 1989, MNRAS, 238, 777
Schmidt M., 1968, ApJ, 151, 393
Sikora M., Stasińska G., Koziel-Wierzbowska D., Madejski G. M., Asari N. V., 2013, ApJ, 765, 62
Simpson C. et al., 2012, MNRAS, 421, 3060
Stott J. P. et al., 2012, MNRAS, 422, 2213
Tremaine S. et al., 2002, ApJ, 574, 740
Tremonti C. A. et al., 2004, ApJ, 613, 898
van Velzen S., Falcke H., Schellart P., Nierstenhöfer N., Kampert K.-H., 2012, A&A, 544, A18
Vikhlinin A. et al., 2009, ApJ, 692, 1033
von der Linden A., Best P. N., Kauffmann G., White S. D. M., 2007, MNRAS, 379, 867
Wen Z. L., Han J. L., 2013, MNRAS, 436, 275
Wen Z. L., Han J. L., 2015a, MNRAS, 448, 2
Wen Z. L., Han J. L., 2015b, ApJ, 807, 178 (WH15)
Wen Z. L., Han J. L., Liu F. S., 2012, ApJS, 199, 34
Willott C. J., Rawlings S., Blundell K. M., Lacy M., 1999, MNRAS, 309, 1017
Zhao J.-H., Burns J. O., Owen F. N., 1989, AJ, 98, 64

SUPPORTING INFORMATION

Additional Supporting Information may be found in the online version of this article:

Table 2. The optical and radio parameters for 7138 radio BCGs. (http://www.mnras.oxfordjournals.org/lookup/suppl/doi:10.1093/mnras/stw1125/-/DC1).

Please note: Oxford University Press is not responsible for the content or functionality of any supporting materials supplied by the authors. Any queries (other than missing material) should be directed to the corresponding author for the article.

This paper has been typeset from a TEX/LATEX file prepared by the author.